ANNALS OF GEOPHYSICS, 68, 4, S450, 2025; doi:10.4401/ag-9285
OPEN ACCESS

Near-Field PSHA with Directivity – Dorud

Behezad Maleki[1], Sayeh Safavi[1], Mohammadreza Najaftomaraei[2], Habib Rahimi[*,1]

(1) Institute of Geophysics, University of Tehran, Tehran, Iran.
(2) Ostim Technical University, Ankara, Turkey

Article history: received February 4, 2025; accepted August 3, 2025

Abstract

This study investigates the probabilistic seismic hazard in Dorud city, located near the active Dorud fault, with a specific focus on incorporating near-field and rupture directivity effects into the hazard modeling framework. Near-field ground motions – particularly those influenced by rupture directivity – can generate long-period velocity pulses, posing serious risks to long-period structures such as bridges and tall buildings near faults. To realistically capture these effects, this study integrates empirical directivity models (Somerville et al., 1997; Abrahamson, 2000) into the probabilistic seismic hazard assessment (PSHA). The seismicity parameters were derived using the Kijko (2004) method based on a carefully declustered earthquake catalog; the suitability of this catalog for PSHA was statistically confirmed through a Kolmogorov-Smirnov (K-S) test, validating the Poissonian nature of inter-event times.Seismic hazard calculations were performed for vibration periods of 0.75, 1, 2, 3, and 4 seconds and return periods of 50, 475, and 2475 years. The study further includes deaggregation analysis to examine how near-field and directivity effects influence magnitude and distance contributions to hazard. The results show that the influence of directivity increases with both return period and vibration period. The most significant amplification – a 17.16% increase in acceleration – occurs when directivity is included for a 2475-year return period at a 4-second vibration period. A regional comparison of seismicity parameters with previous PSHA studies supports the robustness of the selected input values. This study demonstrates the importance of explicitly incorporating directivity in PSHA for fault-adjacent urban areas, especially for engineering design of critical long-period structures.

Keywords: Near-field effect; Directivity; Seismic hazard; Dorud fault

1. Introduction

The Dorud Fault, located at the boundary between the Zagros and Central Iran seismotectonic provinces (Mirzaei et al., 1998), is one of the most seismically active faults in the region. A notable seismic event associated with this fault is the mb 7.4 Silakhor earthquake of January 23, 1909, one of the earliest recorded during the instrumental era (Tchalenko and Braud, 1974; Tchalenko et al., 1974). The fault lies in western Iran, near the cities of Dorud and Broujerd, both of which are significant agricultural centers and popular tourist destinations. The frequent occurrence of microearthquakes in this area provides clear evidence of ongoing seismic activity along the Dorud fault system. Given the seismic hazard posed by this fault, a comprehensive seismic risk assessment is essential.

Such an analysis would not only deepen our understanding... but also enable the estimation of ground motions, accounting for site-specific effects, thereby contributing to the reinforcement of civil structures.

Seismic ground motions near fault zones are often characterized by long-period pulses resulting from the directivity effect, which can severely damage structures, particularly those with long natural periods, such as bridges and dams. Therefore, incorporating the directivity effect into both probabilistic and deterministic seismic hazard assessments is critical for mitigating potential structural damage and reducing fatalities. Numerous studies (e.g., Vader and McDaniel, 2007; Shrestha and Tuladhar, 2012; Adanur et al., 2012) have highlighted the significant impact of near-field ground motion and directivity effects on long-period structures located near highly active strike-slip faults. Various approaches have been employed to model the directivity effect, including analytical methods that examine rupture propagation, rupture direction, and the site's relative position during the ground acceleration time history (Haskell, 1964; Hartzell and Heaton, 1985; Lay and Wallace, 1995). Other studies have analyzed empirical data from near-fault regions to develop relationships that characterize the near-field rupture directivity effect. Notably, Somerville (1997) and Abrahamson (2000) developed widely adopted empirical models for the directivity effect, which are widely used today. Their models consider key parameters such as fault length and the angle between the fault strike and the epicentral direction, as well as their impact on the acceleration spectrum. Somerville et al. (1997) further quantified the directivity effect, and Abrahamson (2000) demonstrated its implications for probabilistic seismic hazard analyses. Building on these models, the present study aims to evaluate the directivity effect on the seismic hazard assessment of the strike-slip Dorud fault system.

2. Seismotectonic of the studied region

Until the Middle Miocene, the interaction between the Iranian and Arabian plates primarily occurred along the Main Zagros Thrust. However, by the end of the Pliocene, a shift in the direction of relative motion between these plates led to the northward movement of the Arabian plate, resulting in convergence toward the Zagros region. The Zagros belt also contains a significant tectonic structure known as the Main Recent Fault (MRF), which runs roughly parallel to the Main Zagros Thrust. The MRF is both younger and more distinct than the Main Thrust and intersects it at several locations (Tchalenko and Braud, 1974). According to Tchalenko and Braud (1974), the MRF is composed of individual right-lateral strike-slip fault segments, often arranged in an en echelon pattern.

The principal segments of the MRF within the study area include the Sahneh Fault, Nahavand Fault, Dorud Fault, and Ardal Fault. Figure 1 illustrates a portion of the MRF along with its major segments and associated significant historical earthquakes (Talebian and Jackson, 2002). These earthquakes are linked to specific fault segments, and the observed right-lateral strike-slip deformation is contemporaneous with late Quaternary deformation in the region (Tchalenko and Braud, 1974). Table 1 lists notable historical earthquakes along the MRF between latitudes 33° and 35°N. Furthermore, the maximum reported displacement along the MRF is 16 km, with an estimated slip rate ranging from 1.6 to 3.2 mm/year (Alipour et al., 2012).

Among the individual segments of the Main Recent Fault (MRF), the Dorud Fault is particularly notable due to its seismic history. This northwest-southeast-trending segment (N315) is nearly vertical and extends approximately 120 km within the Zagros seismotectonic province (Mirzaei et al., 1998). Geological observations have reported right-lateral strike-slip displacements of 10-60 km along the Nahavand and Dorud segments (Gidon et al., 1974). However, Alipour et al. (2012) contended that such displacement did not occur directly along the Dorud segment itself, instead estimating a total displacement of approximately 6 km – considerably less than that observed on other segments of the MRF.

A portion of this displacement, though relatively minor, is attributed to the 1909 Silakhor earthquake (Ms = 7.4), one of the largest seismic events associated with the Dorud Fault segment of the MRF. This earthquake generated dextral (right-lateral) displacements of 0.8-1 meter and vertical displacements of 0.25-0.3 meter (Bachmanov et al., 2004), which contributed to the formation of Lake Gahar (Alipour et al., 2012). The importance of studying the Dorud Fault is further emphasized by Berberian et al. (1976), who proposed that the Silakhor earthquake may have reactivated a section of the MRF.

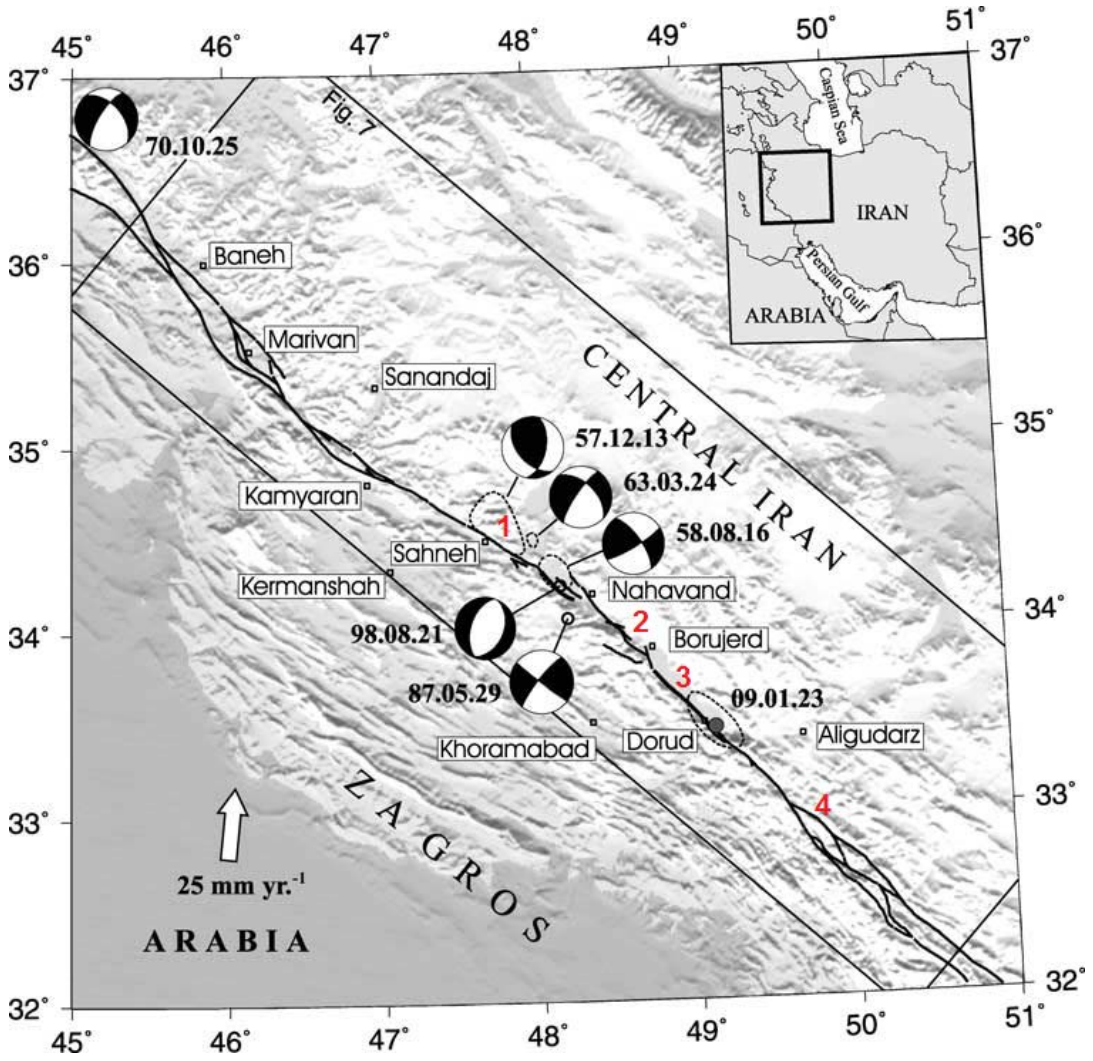

Figure 1. Major fault segments and significant historical earthquakes along the Main Recent Fault in the study area. The numbered segments include: (1) Sahneh Fault; (2) Nahavand Fault; (3) Dorud Fault; and (4) Ardal Fault (Talebian and Jackson, 2002).

Table 1. Notable historical earthquakes associated with the Main Recent Fault.

Date	Lat.	Long.	Ms	Mw	Strike	Dip	Rake	Ref.
1909.01.23	33.41	49.13	7.4	—	—	—	—	A
1957.12.13	34.58	47.82	6.7	—	136	50	50	M
1958.08.16	34.3	48.17	6.6	—	325	70	170	S
1963.03.24	34.5	48.02	5.8	—	314	52	−165	J
1970.10.25	36.77	45.13	4.8	—	319	50	−155	J
1987.05.29	34.05	48.21	—	4.9	128	88	170	H
1998.08.21	34.23	48.16	—	4.9	25	39	−84	H

3. Methodology

3.1 Assessing the Effect of Rupture Directivity on Probabilistic Seismic Hazard Analysis (PSHA)

In this study, the term near-field effects refer to the distinct ground motion characteristics observed when a site is located in close proximity to the earthquake source, typically within a few fault lengths. These effects include large velocity pulses, forward rupture directivity, and a concentration of seismic energy at long periods – factors that are particularly critical for engineering analyses of long-period structures. Although rupture directivity is a primary contributor to near-field effects in strike-slip faults, other phenomena – such as permanent ground displacement, asymmetrical waveforms, and velocity pulse-like behavior – also play a role. Our modeling approach indirectly incorporates these broader near-field characteristics by focusing the hazard assessment on sites near the Dorud Fault (e.g., Dorud1_L. Zone), where such effects are expected to dominate the ground motion response.

Near-fault rupture directivity influences ground motion in two principal ways. First, it affects the overall shaking intensity of the average horizontal ground motion component. Second, it introduces a systematic variation in shaking intensity between the two horizontal components – specifically those aligned perpendicular and parallel to the fault strike.

In this study, we applied the model developed by Somerville et al. (1997), which introduces two period-dependent scaling factors, to strong ground motion attenuation relationships as adapted by Abrahamson (2000). The first scaling factor adjusts for variations in the intensity of the average horizontal ground motion components. These variations result from the directivity effect, wherein rupture propagation toward a site amplifies ground motion, while propagation away from the site diminishes it. The second scaling factor captures the directional characteristics of ground shaking by quantifying the relative intensities of the fault-normal and fault-parallel components with respect to their average.

Abrahamson (2000) further refined the Somerville et al. (1997) model to more accurately represent the average horizontal ground motion component for strike-slip faults, enhancing the scaling of ground motion intensities in the presence of rupture directivity.

$$Ln\ Sa_{Dir}(M,r,x,\theta,T) = Ln\ Sa(M,r) + y_{Dir}(x,\theta,T)T_d(r)T_m(m) \tag{1}$$

Where x is the fault length rupturing toward the site; θ denotes the angle between the strike of the fault and the epicentral azimuth; $T_m(m)$ is the magnitude taper; $T_d(r)$ is the distance taper; $Sa(M,r)$ is an empirical attenuation relation without considering the directivity effect; and $y_{Dir}(x,\theta,T)$ is the directivity function modified by Abrahamson (2000).

The Abrahamson (2000) model was selected for this study due to its explicit treatment of rupture directivity effects within the framework of Probabilistic Seismic Hazard Analysis (PSHA). In contrast to general Ground Motion Prediction Equations (GMPEs), such as Chiou and Youngs (2014), which estimate average ground motions across a broad spectrum of rupture scenarios, Abrahamson's model specifically accounts for the geometry and directionality of rupture propagation. This feature is critical for isolating and analyzing the directivity effect – one of the central focuses of this study. Furthermore, the model builds upon and refines the earlier work of Somerville et al. (1997), which remains widely applied in directivity-sensitive seismic hazard assessments.

To incorporate the directivity effect into Probabilistic Seismic Hazard Analysis (PSHA), the variability introduced by the hypocenter location must be integrated into Eq. (1). Abrahamson (2000) proposed a method specifically designed to incorporate rupture directivity effects into hazard calculations for strike-slip faults. This approach enables a more detailed and accurate assessment of seismic hazard by accounting for the directional influence of rupture propagation on ground motion intensity.

$$v_i(A>z) = N_i(M_{min}) \int_{w=0}^{¥} \int_{RA=0}^{¥} \int_{Ex=0}^{1} \int_{Ey=0}^{1} \int_{hx=0}^{1} \int_{m=M_{min}}^{M_{max}} f_{m_i}(m) f_{W_i}(m,W) f_{RA_i}(m,RA) f_{Ex_i}(x) f_{Ey_i}(m,x)\, f_{h_x}(h_x) P(A>z|m,r,X,\theta) dw dRA dx dy dh_x dm \tag{2}$$

where $N_i(M_{min})$ stands for the rate of earthquakes having a magnitude larger than M_{min} related to the ith source; m denotes the earthquake magnitude; M_{max_i} represents the maximum earthquake magnitude of the ith source;

$f_m(m)$ is the magnitude probability density functions; $f_W(m, W)$ symbolizes the rupture width, and $f_{RA}(m, RA)$ is the rupture area. In addition, f_{EX} and f_{EY} are the location of the center of rupture along strike and down dip, respectively. Moreover, $f_{hx}(h_x)$ denotes the probability density function of the hypocenter location. Finally, $P(A > z|m, r, X, \theta)$ is the probability with which the ground motion surpasses the test level Z for the given magnitude (m), distance (r), and rupture location (θ, X).

3.2 Analysis of Seismicity Parameters in the Study Area

The study area, encompassing the entire Dorud Fault, is defined as a circular region with a diameter of 200 km, centered on the middle segment of the fault. According to Mirzaei et al. (1998), this region spans both the Central Iran and Zagros seismotectonic provinces, which exhibit distinct seismicity characteristics, including differences in b-values and seismicity rates. Accordingly, seismicity parameters were calculated based on the specific location of each seismic source. The contrasting seismic behaviors of these two provinces are illustrated in Fig. 2.

Furthermore, earthquake focal mechanism solutions within the study area are essential for accurately modeling linear seismic sources. To support this modeling effort, we incorporated multiple data sources, including active fault maps from the Encyclopedia of Iran's Faults (2014), the study by Hessami et al. (2003), and focal mechanism solutions for earthquakes with magnitudes greater than 4, as reported by GCMT, HRVD, ISC, and ZUR-RMT (Fig. 3).

In this research, the Probabilistic Seismic Hazard Analysis (PSHA) methodology introduced by Cornell (1968) was applied. A total of 54 seismic sources, including both linear and areal types, were identified across the study area, and their corresponding seismicity parameters were calculated. Specifically, sources were modeled as linear where the fault extent was well-defined or where sufficient information on the focal mechanism solutions of nearby earthquakes was available. In the absence of such information, sources were modeled as areal zones.

The faults within the study region were thus divided into individual segments based on their seismic behavior and faulting mechanisms, with each segment treated as a distinct seismic source. For segments with well-constrained geometries and known focal mechanisms, sources were modeled as finite rectangular fault planes, characterized by parameters such as strike, dip, rake, seismogenic depth, and fault length. For non-vertical faults (i.e., dip $< 90°$), the rupture area and hypocenter distribution were projected along the dipping plane rather than assuming vertical geometry. This more realistic fault representation was incorporated into the PSHA calculations, including directivity

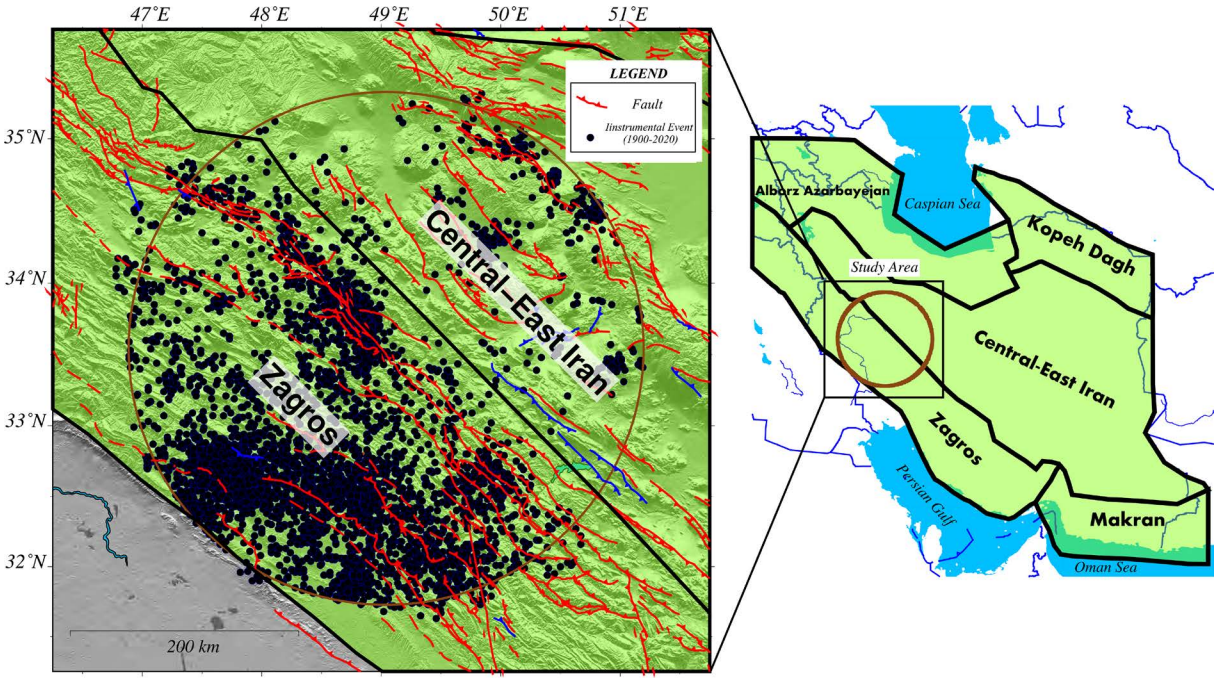

Figure 2. Seismicity of the study region based on the division of Iran's seismotectonic provinces, as defined by Mirzaei et al. (1998).

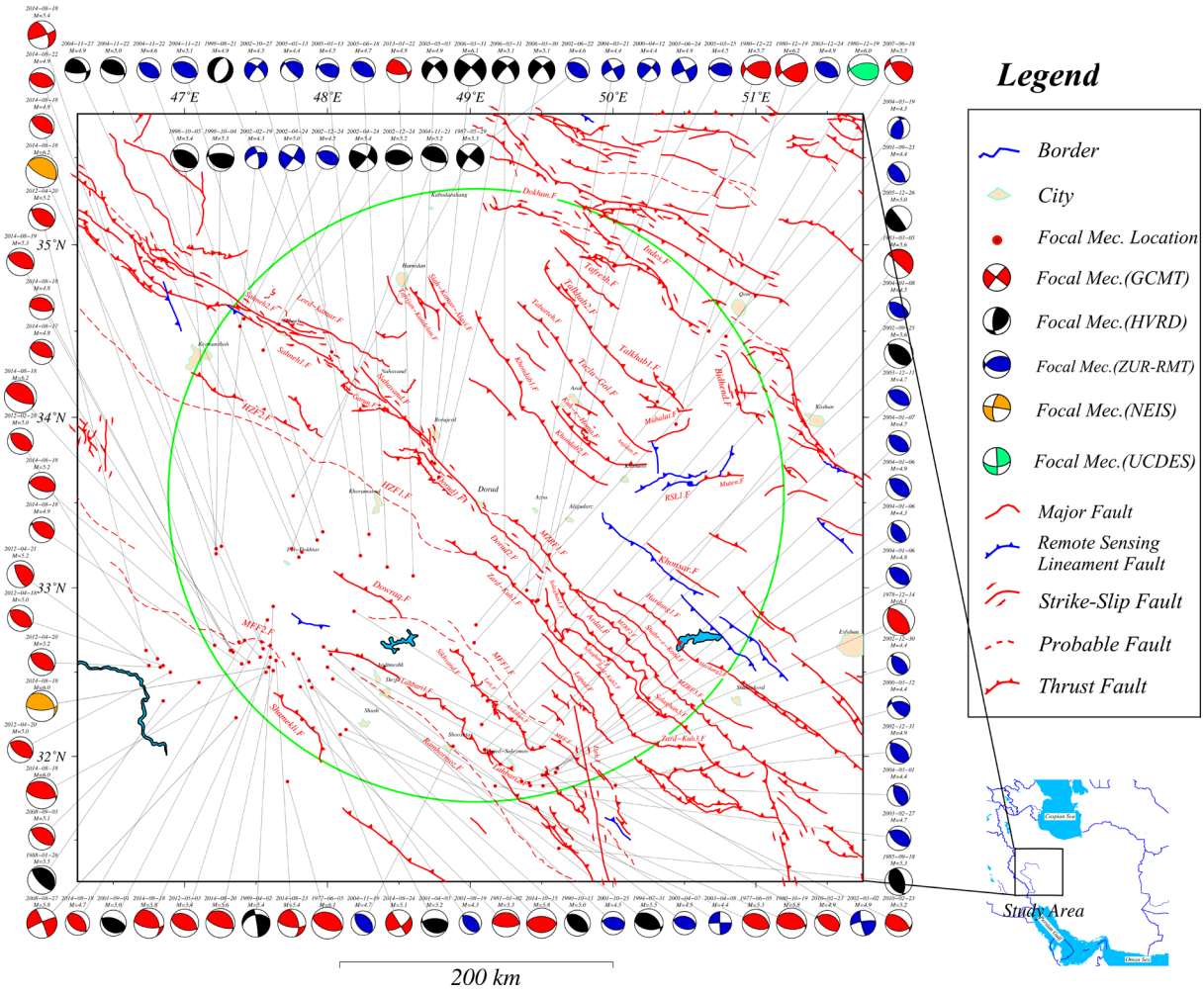

Figure 3. Active faults and focal mechanism solutions of earthquakes with magnitudes greater than 4 (M > 4) within a 200 km radius centered on the middle segment of the Dorud Fault.

modeling based on Abrahamson (2000), which supports non-vertical fault configurations. This approach ensures that fault geometry is accurately reflected in both ground motion prediction and hazard quantification.

Among the 54 seismic sources, two linear sources correspond to segments of the Dorud Fault, designated as Dorud1_L.Zone and Dorud2_L.Zone, as shown in Fig. 4. This figure illustrates the spatial distribution of both linear and areal seismic sources, along with the location of historical and instrumental earthquakes across the study area. Additionally, background seismicity was incorporated within the defined circular region surrounding the fault system.

The parameters for background seismic sources were determined based on earthquakes that occurred outside the delineated linear and areal seismic source zones. Historical earthquakes (pre-1900) and instrumental earthquakes (1900-2012) were compiled using data from Mousavi-Bafrouei et al. (2014). For the period 2012-2019, earthquake data were obtained from the Iranian Seismological Center (IRSC) at the University of Tehran. The completeness magnitude (Mc) of the earthquake catalog was estimated to be 4.3, using the Gutenberg and Richter (1956) method.

To evaluate the influence of different declustering techniques on the earthquake catalog, three established algorithms were applied: Gardner and Knopoff (1974), Uhrhammer (1986), and Grünthal (1998). Figure 5 shows the percentage distribution of earthquake magnitudes in both the original and declustered catalogs. The Y-axis represents the proportion of events within each magnitude bin, rather than absolute event counts. Declustering reduces the number of small-magnitude earthquakes by removing dependent aftershock sequences, which shifts the percentage distribution toward higher magnitudes in some bins. As a result, certain bins in the declustered catalogs may show higher percentages than the original catalog, despite having fewer total events.

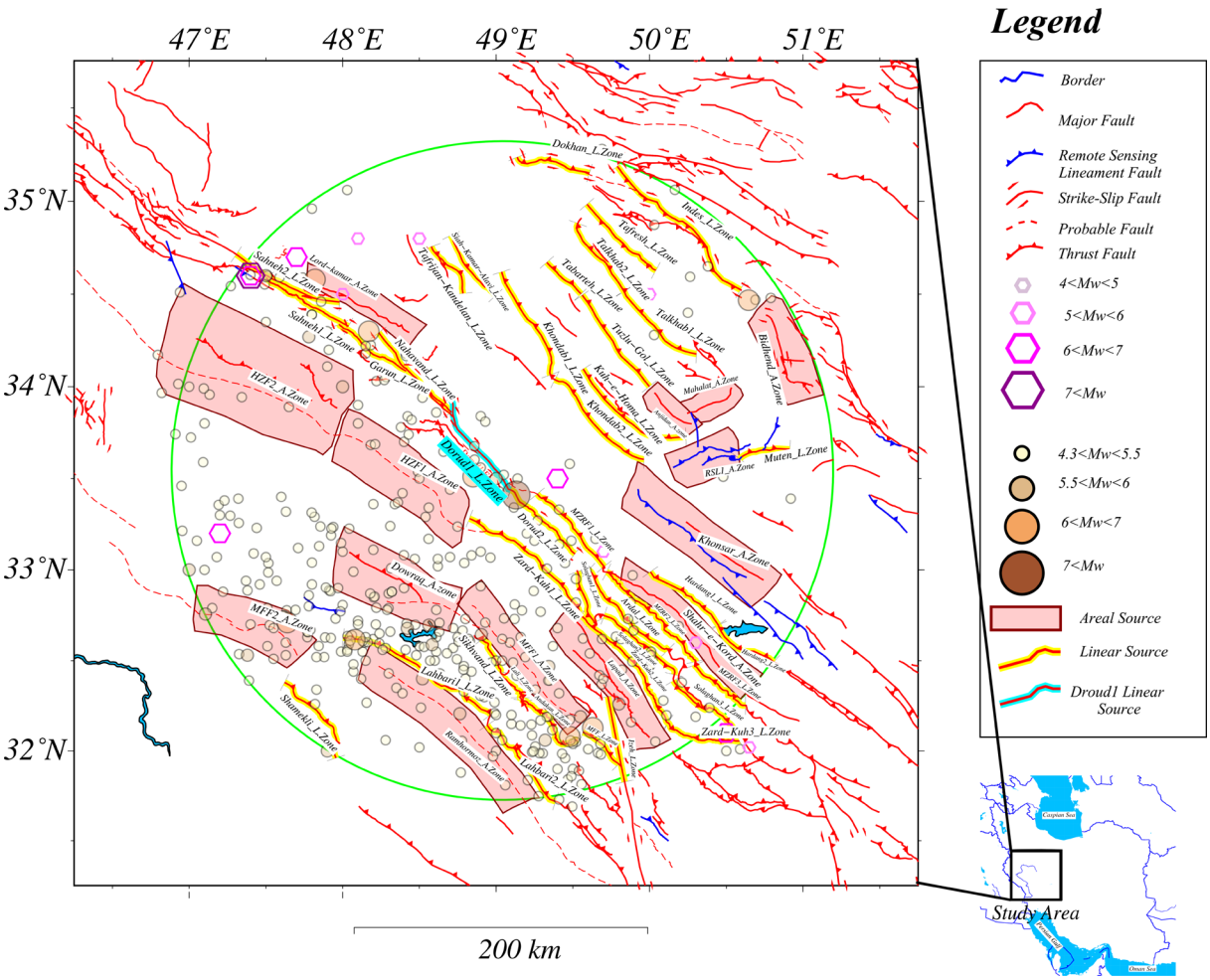

Figure 4. Seismotectonic map of the study region, showing delineated linear and areal seismic sources within a 200 km radius centered on the middle segment of the Dorud Fault. Linear sources (shown in yellow) represent fault segments with well-constrained geometries, while areal sources (shown in pink) correspond to distributed seismic zones where detailed fault information is lacking. The Dorud Fault is highlighted in light blue. Linear sources were modeled as finite rectangular rupture planes using parameters such as strike, dip, and seismogenic depth, and these geometries were incorporated into both the ground motion prediction and directivity modeling framework.

Among the tested methods, the Grünthal (1998) algorithm was selected for further analysis, as it provided a balanced removal of dependent events while retaining sufficient mainshock data. To verify the suitability of the declustered catalog for use in PSHA, a Kolmogorov-Smirnov (K-S) test was conducted on the inter-event times. The test results indicated that the temporal distribution of the declustered events follows a Poisson process (p-value > 0.05), confirming its appropriateness for probabilistic seismic hazard assessment.

Using this approach, a total of 741 dependent earthquake clusters were identified, leaving 1,209 independent events for hazard analysis. Reported earthquake magnitudes and empirical relationships between magnitude and fault length were employed to estimate the maximum magnitude for each seismic source. These relationships were drawn from the studies of Nowroozi (1985), Wells and Coppersmith (1994), and Ambraseys and Jackson (1998). Additionally, fault parameters proposed by Wells and Coppersmith (1994) were applied to the seismic sources identified in this study.

As previously noted, the study area spans two distinct seismotectonic provinces – Central Iran and Zagros – each characterized by unique seismicity behaviors. The key seismicity parameters, including the annual activity rate (λ) and the b-value (β), were estimated separately for each province using the Kijko (2004) method, which integrates both historical and instrumental earthquake data. The results of these calculations are presented in Table 3.

Since the activity rate (λ) is initially determined at the provincial scale, it was subsequently distributed among the individual seismic source zones within each province. For linear sources, the total λ of the respective province

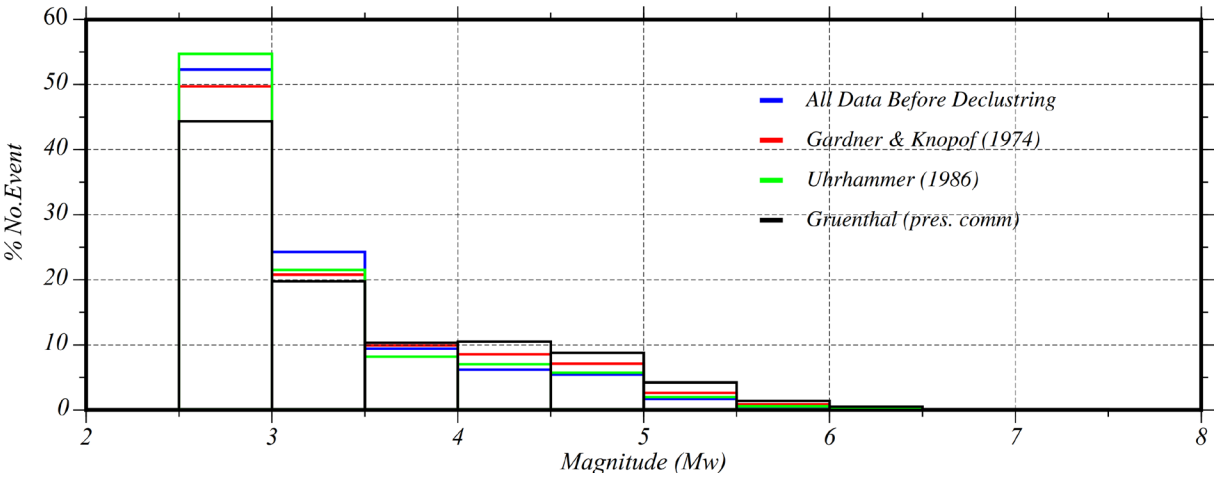

Figure 5. Comparison of the percentage distribution of earthquake magnitudes in the original and declustered catalogs using three declustering methods: Gardner and Knopoff (1974), Uhrhammer et al. (1986), and Grünthal (1998). The Y-axis represents the percentage of events in each magnitude bin relative to the total in each version of the catalog. Declustering removes clusters of small-magnitude events, reshaping the distribution toward higher relative proportions in larger magnitude bins. The Grünthal method was selected for this study, and a Kolmogorov-Smirnov (K-S) test confirmed that the resulting catalog follows a Poissonian temporal distribution ($p > 0.05$).

was apportioned based on the length of each fault segment, assuming a uniform distribution of seismicity along strike. For areal sources, λ was distributed proportionally to the surface area of each zone. This approach provides a consistent and regionally informed estimation of seismicity input parameters for use in the PSHA.

To place the seismicity parameters used in this study within a broader regional context, Table 4 presents a comparison with selected PSHA studies previously conducted in Iran. As shown, the b-values, maximum magnitudes, and activity rates applied in this analysis fall within the range of values reported in the literature, thereby supporting the regional validity and robustness of the seismic source characterization employed in this study.

Table 2. Calculated annual rates of earthquakes (λ), β, and maximum magnitude (M_{max}) for each seismotectonic province of the studied region.

Seismotectonic Province	M_{max}	β	λ
Zagros	7.65	2.52	10.360 (for $M_{min} = 4.3$ M_w)
Central Iran	5.85	2.39	1.615 (for $M_{min} = 4.3$ M_w)

Table 3. Estimated seismicity parameters for the linear and areal seismic source zones in the study region. The b-values and maximum magnitudes were calculated using the Kijko (2004) method, combining historical and instrumental data. Annual activity rates (λ) were first determined at the seismotectonic province level and then proportionally distributed among individual source zones based on fault length (for linear sources) or surface area (for areal zones).

No.		Fault Zone Name	Seismotectonic Province	Det. Mag.	Seismogenic Depth	Dip	Min. Mag.	Beta	Activity Rate	Fault Length
1	Line Source	Andakan_F.Zone	Zagros	6.8	5 to 20	5	4.3	2.53	0.212	55.7
2		Ardal_F.Zone	Zagros	6.9	5 to 20	45	4.3	2.53	0.274	72.1
3		Dokhan_F.Zone	Central Iran	6.7	5 to 20	45	4.3	2.53	0.177	46.64
4		Dorud1_F.Zone	Zagros	6.9	5 to 20	70	4.3	2.53	0.273	71.9
5		Dorud2_F.Zone	Zagros	7.4	5 to 20	70	4.3	2.53	0.218	57.3
6		Garun_F.Zone	Zagros	6.7	5 to 20	90	4.3	2.53	0.193	50.8
7		Hardang1_F.Zone	Zagros	6.8	5 to 20	45	4.3	2.53	0.206	54.2
8		Hardang2_F.Zone	Central Iran	6.7	5 to 20	45	4.3	2.53	0.164	43.1
9		Indes_F.Zone	Central Iran	7.1	5 to 20	53	4.3	2.53	0.412	108.5
10		Izeh_F.Zone	Zagros	6.8	5 to 20	61	4.3	2.53	0.203	53.4
11		Khondab1_F.Zone	Central Iran	6.9	5 to 20	45	4.3	2.53	0.268	70.6
12		Khondab2_F.Zone	Zagros	6.9	5 to 20	45	4.3	2.53	0.285	74.9
13		Kuh-e-Homa_F.Zone	Central Iran	6.9	5 to 20	45	4.3	2.53	0.303	79.7
14		Lahbari1_F.Zone	Zagros	7.1	5 to 20	30-60	4.3	2.53	0.408	107.4
15		Lahbari2_F.Zone	Zagros	6.9	5 to 20	30-60	4.3	2.53	0.252	66.4
16		Lali_F.Zone	Zagros	6.3	5 to 20	5	4.3	2.53	0.085	22.21
17		MFF_F.Zone	Zagros	6.5	5 to 20	40	4.3	2.53	0.114	30
18		Muten_F.Zone	Central Iran	6.5	5 to 20	45	4.3	2.39	0.079	31.84
19		MZRF1_F.Zone	Zagros	6.8	5 to 20	45	4.3	2.53	0.234	61.4
20		MZRF2_F.Zone	Zagros	7.0	5 to 20	45	4.3	2.53	0.32	84.1
21		MZRF3_F.Zone	Zagros	6.7	5 to 20	45	4.3	2.53	0.164	43.13
22		Nahavand_F.Zone	Zagros	6.9	5 to 20	90	4.3	2.53	0.251	65.9
23		Sahneh1_F.Zone	Zagros	6.8	5 to 20	90	4.3	2.53	0.227	59.6
24		Sahneh2_F.Zone	Zagros	6.9	5 to 20	90	4.3	2.53	0.263	69.1
25		Shamekli_F.Zone	Zagros	6.8	5 to 20	30-60	4.3	2.53	0.235	61.8
26		Siah-Kamar-Alavi_F.Zone	Central Iran	6.7	5 to 20	45	4.3	2.39	0.113	45.69

No.		Fault Zone Name	Seismotectonic Province	Det. Mag.	Seismogenic Depth	Dip	Min. Mag.	Beta	Activity Rate	Fault Length
27	Line Source	Sikhvand_F.Zone	Zagros	6.4	5 to 20	5	4.3	2.53	0.095	24.81
28		Solaghan1_F.Zone	Zagros	6.5	5 to 20	41	4.3	2.53	0.128	33.66
29		Solaghan2_F.Zone	Zagros	6.8	5 to 20	41	4.3	2.53	0.223	58.6
30		Solaghan3_F.Zone	Zagros	6.7	5 to 20	41	4.3	2.53	0.192	50.4
31		Tabarteh_F.Zone	Central Iran	6.4	5 to 20	59	4.3	2.39	0.07	28.13
32		Tafresh_F.Zone	Central Iran	6.8	5 to 20	59	4.3	2.39	0.143	58
33		Tafrijan-Kandelan_F.Zone	Central Iran	6.6	5 to 20	45	4.3	2.39	0.089	36.2
34		Talkhab1_F.Zone	Central Iran	6.8	5 to 20	59	4.3	2.39	0.147	59.5
35		Talkhab2_F.Zone	Central Iran	6.7	5 to 20	59	4.3	2.39	0.125	50.8
36		Tuzlu-Gol_F.Zone	Central Iran	6.9	5 to 20	59	4.3	2.39	0.169	68.5
37		Zard-Kuh1_F.Zone	Zagros	7.0	5 to 20	33-60	4.3	2.53	0.35	92
38		Zard-Kuh2_F.Zone	Zagros	7.0	5 to 20	33-60	4.3	2.53	0.339	89.2
39		Zard-Kuh3_F.Zone	Zagros	6.7	5 to 20	30-60	4.3	2.53	0.186	49
40	Area Source	Anjidan_A.zone	Central Iran	6.6	5 to 20	—	4.3	2.39	0.09	36.3
41		Bidhend_A.Zone	Central Iran	6.8	5 to 20	—	4.3	2.39	0.156	63.2
42		Dowraq_A.zone	Zagros	6.9	5 to 20	—	4.3	2.53	0.294	77.3
43		Gavmir_A.Zone	Zagros	6.9	5 to 20	—	4.3	2.53	0.26	68.5
44		HZF1_A.Zone	Zagros	7.0	5 to 20	—	4.3	2.53	0.348	91.5
45		HZF2_A.Zone	Zagros	7.1	5 to 20	—	4.3	2.53	0.435	114.6
46		Khonsar_A.Zone	Central Iran	7.1	5 to 20	—	4.3	2.39	0.26	105.6
47		Lapad_A.Zone	Zagros	7.1	5 to 20	—	4.3	2.53	0.379	99.7
48		Lord-kamar_A.Zone	Zagros	6.9	5 to 20	—	4.3	2.53	0.284	74.8
49		Mahalat_A.Zone	Central Iran	6.5	5 to 20	—	4.3	2.39	0.078	31.4
50		MFF1_A.Zone	Zagros	7.1	5 to 20	—	4.3	2.53	0.406	106.8
51		MFF2_A.Zone	Zagros	6.9	5 to 20	—	4.3	2.53	0.273	71.75
52		Ramhormoz_A.Zone	Zagros	7.2	5 to 20	—	4.3	2.53	0.497	130.82
53		RSL1_A.Zone	Central Iran	6.6	5 to 20	—	4.3	2.39	0.105	42.44
54		Shahr-e-Kord_A.Zone	Zagros	7.1	5 to 20	—	4.3	2.53	0.406	106.9
55		Backgorund_Seismicity	—	6.3	5 to 20	—	4.3	2.39	1.615	—

Table 4. Comparison of key seismicity parameters (b-values, maximum magnitude, and activity rate) used in this study with those reported in selected regional PSHA studies in Iran. This comparison supports the regional validity and consistency of the adopted values.

Study / Source	Region Covered	b-value (β)	M_{max}	Activity Rate (λ) (events/year)	Notes
This study	Zagros & Central Iran	2.39-2.53	5.85-7.65	1.615-10.360	Based on updated declustered catalog
Mirzaei et al. (1998)	National (Iran-wide)	~2.4	~7.5	Not reported	Source zonation and seismotectonics
Zare et al. (2014)	Zagros	2.5	7.5-7.7	~8-12	NGA-West based PSHA
Mousavi-Bafrouei et al. (2014)	Iran Plateau (declustered)	~2.4	6.8-7.5	~3-10	Updated declustered catalog
Ambraseys & Jackson (1998)	Eastern Mediterranean & Iran	—	7.4-7.6	—	Based on historical events

4. Discussion and Conclusion

4.1 The Effect of Directivity on the Seismic Hazard Curve of the Dorud Fault

Seismic hazard curves are used to evaluate the probability of earthquake occurrence within a seismic source and to quantify the expected ground motion parameters. To investigate the near-field directivity effects in the city of Dorud, a representative site located at latitude 33.725° and longitude 48.781°, near the first seismic source zone of the Dorud Fault (Dorud1_L.Zone), was selected. This zone plays a critical role in controlling ground motion behavior associated with the Dorud Fault system. The seismic hazard at this site, incorporating the directivity effect, was calculated using the methodology developed by Abrahamson (2000).

Figure 6 presents the seismic hazard curves with and without the inclusion of the directivity effect for spectral periods of 1 second and 2 seconds. The results indicate that as the earthquake return period increases, the ground

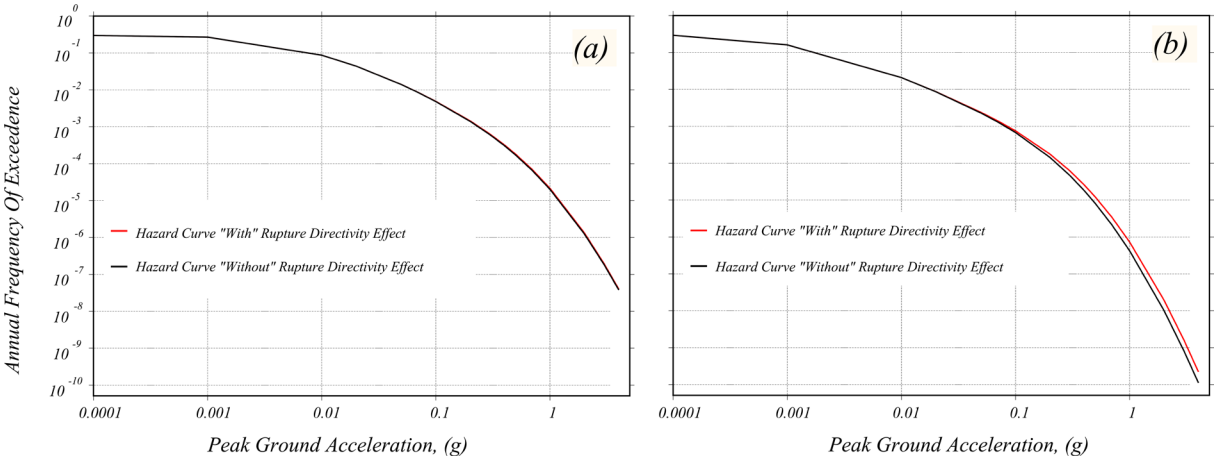

Figure 6. Seismic hazard curves for the Dorud1_L.Zone at spectral periods of (a) 1 second and (b) 2 seconds, showing ground motion values for various return periods with and without the incorporation of the rupture directivity effect.

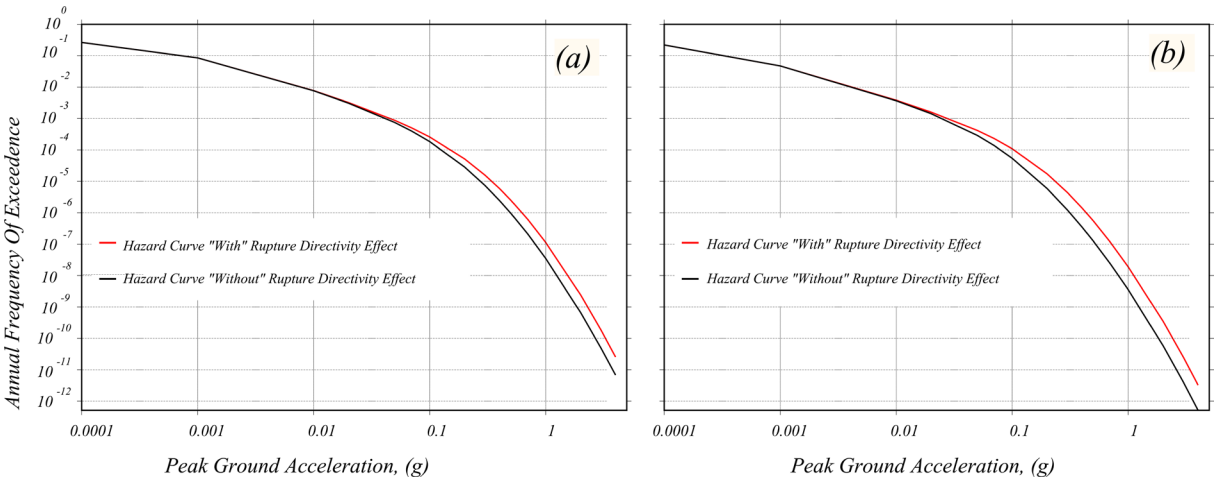

Figure 7. Seismic hazard curves for the Dorud1_L.Zone at spectral periods of (a) 3 seconds and (b) 4 seconds, illustrating ground motion values for various return periods with and without the inclusion of the rupture directivity effect.

acceleration values computed with the directivity effect show a more pronounced increase compared to those without it. A similar trend is observed for 3-second and 4-second periods, as shown in Fig. 7.

Moreover, a comparison of the hazard curves across 1- to 4-second periods (Figs. 6 and 7) reveals that the impact of rupture directivity becomes increasingly significant with longer spectral periods. This highlights the importance of accounting for directivity in the probabilistic seismic hazard assessment of long-period structures located near active strike-slip faults like the Dorud Fault.

Therefore, it can be concluded that both the vibration period and the earthquake return period influence how the directivity effect manifests in probabilistic seismic hazard assessments (PSHA). While the inclusion of directivity has minimal impact on low-return-period or short-period structures, its effect becomes more noticeable for long-period ground motions (e.g., 3-4 sec) and longer return periods (e.g., 475-2475 years). For example, as shown in Table 4, the acceleration increase due to directivity reaches up to 17.16% for a 4-second vibration period at a 2475-year return period. Although this may appear modest in average hazard curves, it becomes critical in performance-based seismic design and code-level applications for long-period structures near active faults.

4.2 The Effect of Directivity on Strong Ground Motion Acceleration

Incorporating near-fault rupture directivity effects into seismic hazard analysis is crucial for accurately estimating strong ground motion acceleration, which directly informs the development of structural design codes and standards for civil infrastructure. In this study, we quantitatively analyzed the influence of rupture directivity on ground acceleration near the Dorud Fault. Specifically, acceleration parameters were examined over a 3-second spectral period for various earthquake recurrence intervals. Additionally, the variation in acceleration – with and without consideration of directivity – was assessed across multiple spectral periods.

At a representative site near the Dorud Fault, located at latitude 33.725° and longitude 48.781°, acceleration values were computed for periods greater than 0.75 seconds corresponding to return periods of 10, 50, 75, 145, 475, 950, and 2475 years, incorporating the directivity effect (see Table 5). As shown in Table 5, acceleration generally increases with both spectral period and recurrence interval. This trend reflects the greater accumulation of stress along the fault over longer return periods, increasing the likelihood of larger magnitude earthquakes. These findings are consistent with those of Somerville (2003), who demonstrated that the directivity effect intensifies with increasing earthquake magnitude.

Furthermore, acceleration values across different spectral periods – both including and excluding the directivity effect – were computed for multiple return periods and are presented in Fig. 8. The results indicate that the directivity effect on strong ground motion acceleration becomes more pronounced at longer periods, exerting a greater influence on long-period ground motions compared to short-period motions.

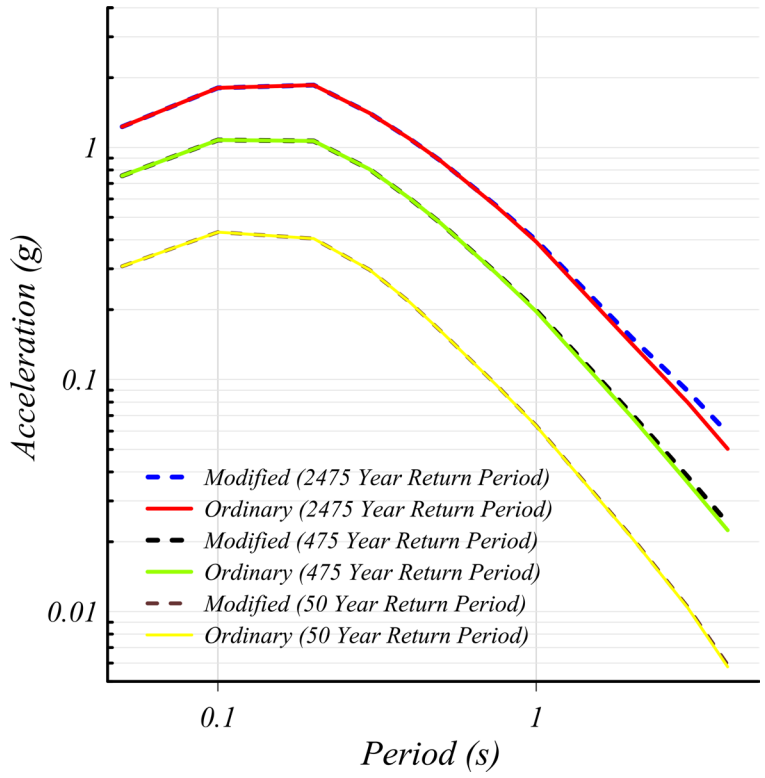

Figure 8. Assessment of strong ground motion acceleration for return periods of 50, 475, and 2475 years, with (dashed lines) and without (solid lines) the incorporation of the rupture directivity effect.

Table 5. Percentage increase in strong ground motion acceleration across different spectral periods and return periods due to the incorporation of the rupture directivity effect, based on the model by Abrahamson (2000).

The acceleration percentage increase for several periods in different return periods (Latitude: 33.725, Longitude: 48.871) (%)							
Period (sec)	**10 years**	**50 years**	**75 years**	**145 years**	**475 years**	**950 years**	**2475 years**
0.75	00.028	00.138	00.171	00.307	00.454	00.571	00.592
1	00.042	00.285	00.394	00.633	01.170	01.316	01.581
2	00.125	00.577	00.965	01.644	03.033	04.349	06.180
3	00.441	00.773	01.375	02.294	05.987	07.786	12.098
4	00.691	01.904	02.231	03.080	07.445	12.317	17.160

Seismic hazard maps were generated for the region bounded by 32.8°-34.2° latitude and 48.2°-50.1° longitude, illustrating strong ground motion acceleration with and without the rupture directivity effect for return periods of 50, 475, and 2475 years, all corresponding to a 3-second spectral period (Figs. 9, 10 and 11). As shown in Fig. 9, the impact of directivity is minimal for the shorter 50-year return period. However, its influence becomes progressively more pronounced for the 475-year (Fig. 10) and especially the 2475-year return period (Fig. 11).

It is noteworthy that, as previously indicated in Fig. 8 and Table 5, the relative increase in spectral acceleration due to directivity becomes more substantial with longer return periods – particularly at longer vibration periods.

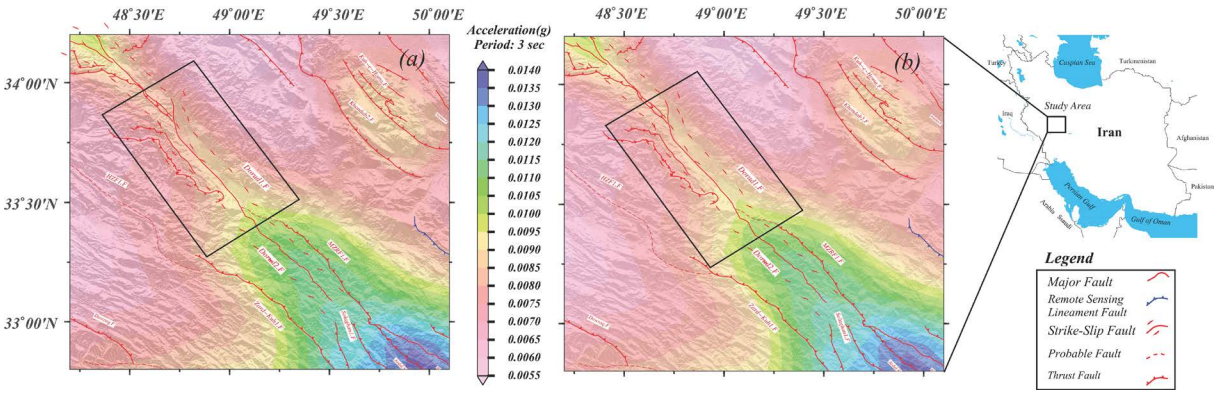

Figure 9. Seismic hazard map of the study region near the Dorud Fault for a 50-year return period at a 3-second spectral period: (a) with the incorporation of the rupture directivity effect and (b) without it.

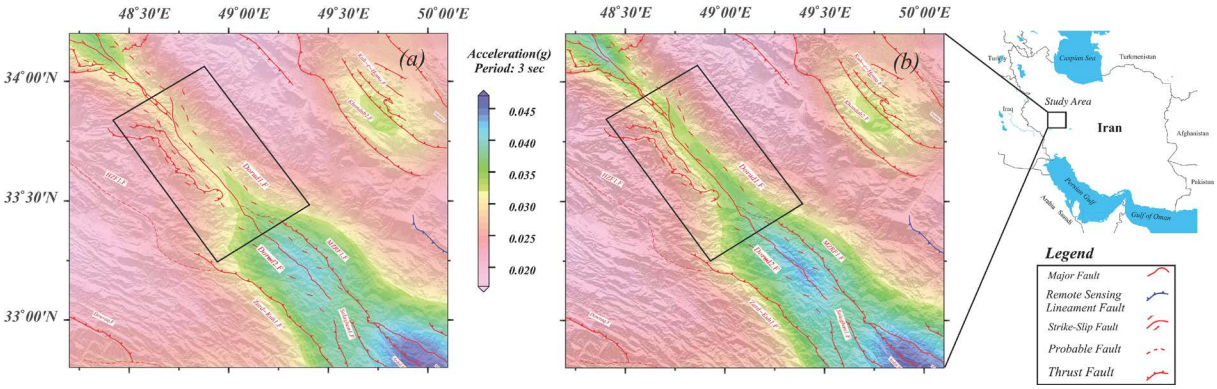

Figure 10. Seismic hazard map of the study region near the Dorud Fault for a 475-year return period at a 3-second spectral period: (a) with the incorporation of the rupture directivity effect and (b) without it.

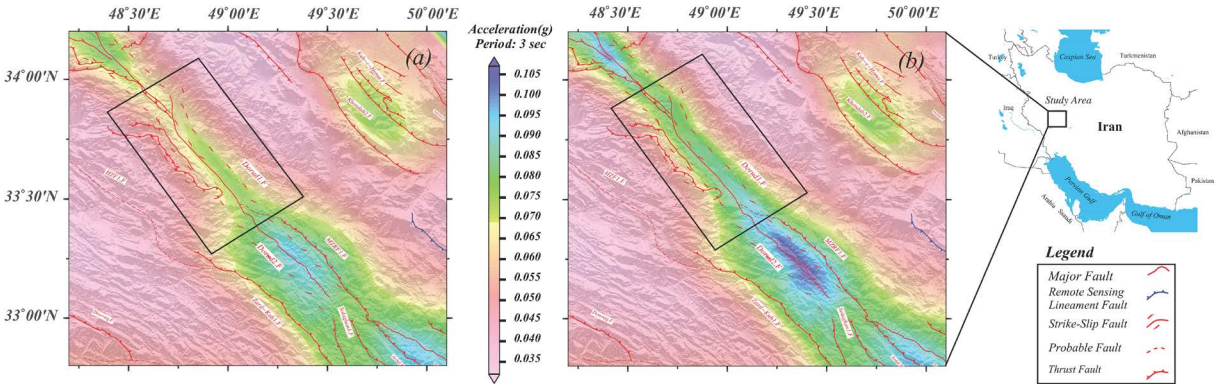

Figure 11. Seismic hazard map of the study region near the Dorud Fault for a 2475-year return period at a 3-second spectral period: (a) with the incorporation of the rupture directivity effect and (b) without it.

Figures 12 and 13 further illustrate this trend by providing spatial plots that emphasize the 475-year return period, where the concentration of energy release – and thus the amplification due to directivity – is most visually apparent.

For longer return periods (e.g., 975 or 2475 years), although numerical differences in spectral acceleration remain significant (especially at T = 4 s), the spatial distribution of potential rupture scenarios becomes more diffuse. Consequently, the visual contrast between hazard maps with and without directivity diminishes. This observation highlights a critical distinction between localized amplification patterns caused by rupture directivity and broader hazard surface trends, a nuance further discussed in the subsequent analysis.

4.3 Discussion and Conclusion: The Effect of Directivity on Seismic Hazard Deaggregation Strong Ground Motion Acceleration

In probabilistic seismic hazard assessment (PSHA), seismic hazard is quantified based on the likelihood of earthquakes of varying magnitudes and distances affecting a specific site. Seismic hazard deaggregation enables the analysis of these contributions by computing the probability density functions (PDFs) for different magnitude-distance pairs. In this study, deaggregation was performed for a site near the Dorud Fault (latitude 33.725°, longitude 48.781°) for return periods of 50, 475, and 2475 years, at a 3-second spectral period, both with and without the incorporation of the rupture directivity effect.

Figure 12 presents the probability density functions for the distance contribution to ground motion. For the 50-year return period (Fig. 12a), the directivity effect had no observable impact on the deaggregation results. However, at the 475-year return period (Fig. 12b), the influence of directivity became more apparent, significantly increasing the contribution of sources close to the fault, while distant contributions remained largely unaffected. At the 2475-year return period (Fig. 12c), the influence of directivity was again less pronounced than at 475 years, due to the more distributed nature of likely rupture scenarios.

Similarly, Fig. 13 illustrates the contribution of magnitude to ground motion. For the 50-year return period (Fig. 13a), directivity had no significant influence. At the 475-year return period (Fig. 13b), however, directivity noticeably affected contributions from moderate magnitude events, amplifying their influence on ground motion. At 2475 years (Fig. 13c), the effect of directivity on magnitude contribution was again relatively minor, likely due to the dominance of large-magnitude events over rupture geometry in determining hazard levels.

These findings are consistent with the expected behavior of rupture directivity in strike-slip faults, where long-period ground motion pulses are generated and have a disproportionately large impact on structures with long natural periods – including bridges, dams, and high-rise buildings. The Somerville et al. (1997) and Abrahamson (2000) models used in this analysis are specifically designed to account for such directivity effects and were appropriately applied to the Dorud Fault, a major strike-slip structure.

The comparison of deaggregation results across return periods revealed that:

- At 50 years, distance and magnitude contributions were not significantly affected by directivity.
- At 475 years, directivity altered both distance and magnitude contributions, emphasizing the importance of near-fault sources and moderate-magnitude events.
- At 2475 years, the influence of directivity was again reduced, reflecting the overriding impact of high-magnitude events distributed over a wider area.

Notably, the inclusion of directivity increased ground acceleration as both the period and return period grew. The maximum observed impact was a 17.16% increase in acceleration at a 4-second period for the 2475-year return period. These findings are critical, as long return periods are directly used in seismic design regulations such as ASCE 7-05, ASCE 7-10, and the International Building Code (IBC). Incorporating directivity into PSHA models, therefore, has practical value for improving design safety and resilience of long-period structures.

While this study focuses on directivity as a key near-field phenomenon, it should be noted that the broader category of near-field effects was also inherently addressed through both site selection and the use of empirical models (e.g., Somerville et al., 1997; Abrahamson, 2000), which were developed using near-fault strong motion data. These models naturally account for pulse-like motions, permanent displacements, and other near-field features.

Although directivity introduces less epistemic uncertainty than other factors – such as fault slip rates or the b-value in magnitude-frequency relationships – it plays a critical role in shaping and amplifying long-period ground motions. Given the sensitivity of vital infrastructure to these motions, even modest statistical differences in hazard estimates can translate into substantial differences in seismic design outcomes. Thus, including rupture directivity in hazard modeling is not only justified but necessary for effective risk mitigation near active strike-slip faults.

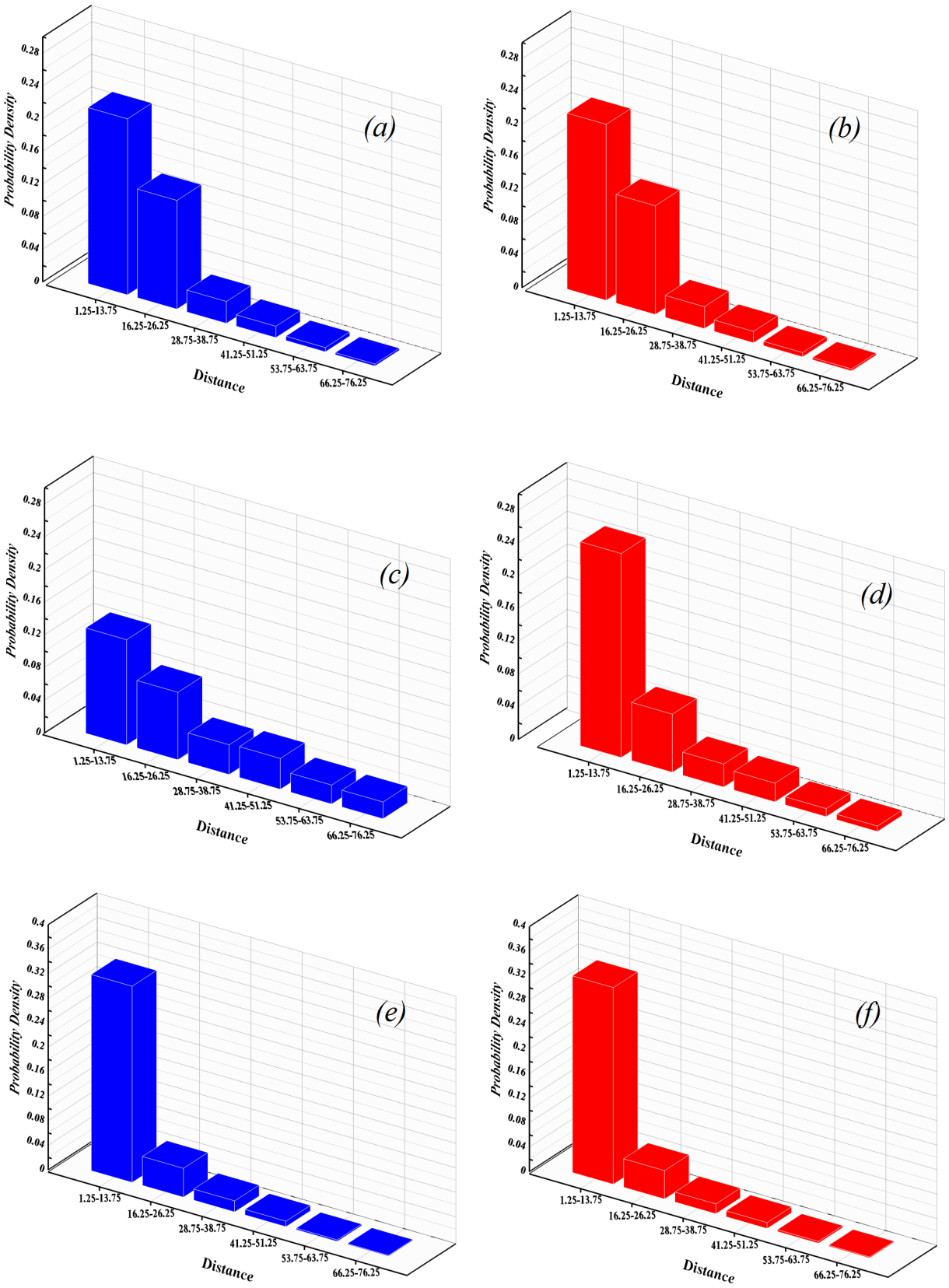

Figure 12. Deaggregation results for a point near the Dorud Fault (latitude 33.725°, longitude 48.781°), showing the contribution of distance to strong ground motion acceleration with (blue bars) and without (red bars) the directivity effect: (a) and (b) for the 50-year return period; (c) and (d) for the 475-year return period; and (e) and (f) for the 2475-year return period.

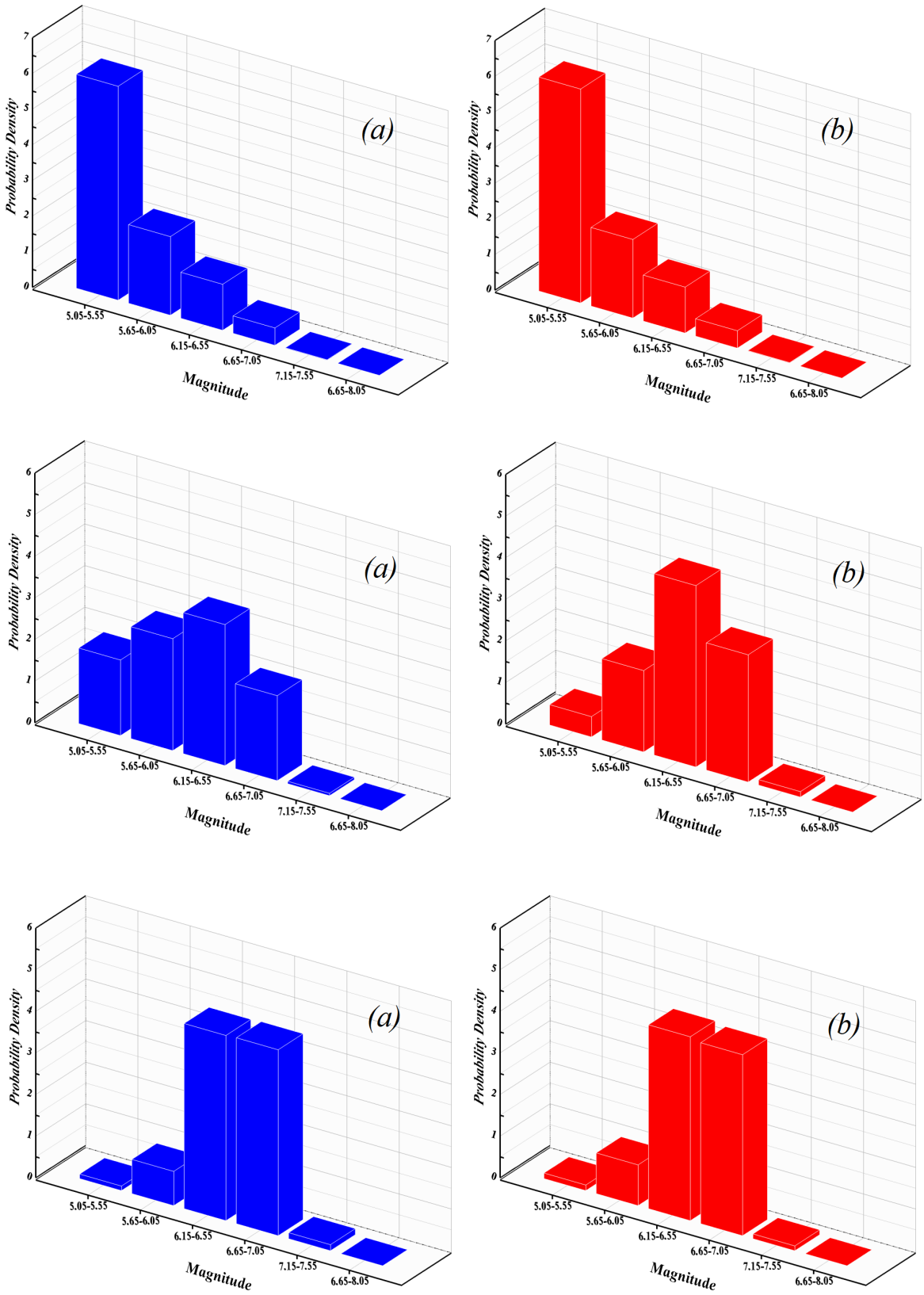

Figure 13. Deaggregation results for a point near the Dorud Fault (latitude 33.725°, longitude 48.781°), showing the contribution of magnitude to strong ground motion acceleration with (blue bars) and without (red bars) the directivity effect: (a) and (b) for the 50-year return period; (c) and (d) for the 475-year return period; and (e) and (f) for the 2475-year return period.

Data availability statement. The data used in this study can be accessed by email.

Acknowledgements. The authors gratefully acknowledge the Iranian Seismological Center (IRSC) and the International Institute of Earthquake Engineering and Seismology (IIEES) for providing the historical and instrumental earthquake catalogs used in this study. These data formed the essential foundation for the seismic source characterization and hazard analysis presented in this work.

References

Abrahamson, N. A. (2000). Effects of rupture directivity on probabilistic seismic hazard analysis. In Proc. 6th Int. Conf. Seismic Zonation, Palm Springs, CA, 12-15 November 2000, Earthquake Engineering Research Institute.

Adanur, S., A. C. Altunişik and A. Bayraktar (2012). Comparison of near-fault and far-fault ground motion effects on geometrically nonlinear earthquake behavior of suspension bridges, Nat. Hazards, 64, 593-614.

Alipour, R., M. Zare and M. R. Ghassemi (2012). Inception of activity and slip rate on the Main Recent Fault of Zagros Mountains, Iran, Geomorphology, 175-176, 86-97.

Ambraseys, N. N. and C. P. Melville (1982). A History of Persian Earthquakes, Cambridge University Press.

Ambraseys, N. N. and J. A. Jackson (1998). Faulting associated with historical and recent earthquakes in the eastern Mediterranean region, Geophys. J. Int., 133, 390-406.

Bachmanov, D. M., V. G. Trifonov, Kh. T. Hessami, T. P. Kozhurin et al. (2004). Active faults in the Zagros and central Iran, Tectonophysics, 380, 221-241.

Berberian, M. (1976). Contribution on the Seismotectonics of Iran: Part I. Geological Survey of Iran, Tehran, 517.

Berberian, M. (1981). Active faulting and tectonics of Iran, in H. K. Gupta and F. M. Delany (Eds.), Zagros-Hindu Kush-Himalaya Geodynamic evolution 33-69, Am. Geophys. Union.

Campbell, K. W. and Y. Bozorgnia (2014). NGA-West2 ground motion model for the average horizontal components of PGA, PGV, and 5% damped linear acceleration response spectra, Earthquake Spectra, 30, 3, 1087-1115.

Chiou, B. S.-J. and R. R. Youngs (2014). Update of the Chiou and Youngs NGA model for the average horizontal component of peak ground motion and response spectra, Earthquake Spectra, 30, 3, 1117-1153.

Cornell, C. A. (1968). Engineering seismic risk analysis. Bull. Seismol. Soc. Am., 58, 5, 1583-1606.

Gardner, J. K. and L. Knopoff (1974). Is the sequence of earthquakes in Southern California, with aftershocks removed, Poissonian? Bull. Seismol. Soc. Am., 64, 5, 1363-1367.

Gidon, M., F. Berthier, J. P. Billiault, B. Halbronn et al. (1974). Sur le caractère et l'ampleur du coulissement de la 'Main Fault' dans la région de Borujerd-Dorud, Zagros oriental, Iran. C. R. Acad. Sci. Paris, Série D, 278, 701-704.

Grünthal, G. (1998). European Macroseismic Scale 1998 (EMS-98), Cah. Cent. Eur. Géodyn. Séismol., 15, Centre Européen de Géodynamique et de Séismologie, Luxembourg.

Haskell, N. (1964). Total energy and energy spectral density of elastic wave radiation from propagating faults, Bull. Seismol. Soc. Am., 56, 1811-1842.

Harzell, S. H. and T. H. Heaton (1985). Teleseismic time function for large, shallow subduction zone earthquake, Bull. Seismol. Soc. Am., 75, 965-1004.

Hessami, K., F. Jamali and H. Tabassi (2003). Major active faults of Iran, scale 1:2,500,000, Int. Inst. Earthquake Eng. Seismol.

Idriss, I. M. (2014). An NGA-West2 empirical model for estimating the horizontal spectral values generated by shallow crustal earthquakes, Earthquake Spectra, 30, 3, 1155-1177.

Jackson, J. A. (1980). Reactivation of basement faults and crustal shortening in orogenic belts, Nature, 283, 343-346.

Jackson, J. and T. Fitch (1981). Basement faulting and the focal depths of the larger earthquakes in the Zagros Mountains (Iran), Geophys. J. R. Astron. Soc., 64, 561-586.

Kamai, R., N. A. Abrahamson and W. J. Silva (2014). Nonlinear horizontal site amplification for constraining the NGA-West2 GMPEs, Earthquake Spectra, 30, 3, 1223-1240.

Kijko, A. (2004). Estimation of the maximum earthquake magnitude, M_{max}, Pure Appl. Geophys., 161, 8, 1655-1681.

Lay, T. and T. Wallace (1995). Modern Global Seismology. Academic Press.

Maleki, B., H. Rahimi and V. Maleki (2019). Applying the characteristic magnitude distribution model for North Tabriz Fault (NTF) in probabilistic seismic hazard assessment (PSHA) and its effects on acceleration parameter and hazard curve. J. Earth Space Phys., 45, 3, 4.

McKenzie, D. P. (1972). Active tectonics of the Mediterranean region, Geophys. J. R. Astron. Soc., 30, 109-185.
McKenzie, D. P. and J. A. Jackson (1983). The relation between strain rates, crustal thickening, paleomagnetism, finite strain and fault movements within a deforming zone, Earth Planet. Sci. Lett., 65, 182-202.
Mirzaei, N., M. Gao and Y. T. Chen (1998). Seismic source regionalization for seismic zoning of Iran: Major seismotectonic provinces, J. Earthquake Predict. Res., 7, 465-495.
Molnar, P. and W. P. Chen (1982). Seismicity and mountain building, in K. J. Hsu (Ed.), Mountain Building Processes, 41-57, Academic Press.
Mousavi-Bafrouei, S. H., N. Mirzaei and E. Shabani (2014). A declustered earthquake catalog for Iranian plateau. Ann. Geophys., 57, 6, S653, doi:10.4401/ag-6395.
Nowroozi, A. A. (1985). Empirical relations between magnitudes and fault parameters for earthquakes in Iran, Bull. Seismol. Soc. Am., 75, 5, 1327-1338.
Shahvar, M. P., M. Zar and S. Castellaro (2013). A unified seismic catalog for the Iranian plateau (1900-2011), Seismol. Res. Lett., 84, 233-249.
Shaykh al-Islami, M. R., H. Javadi, M. Asadi-Sarshar, A. Aqahoseyni et al. (2015). Encyclopedia of Iranian Faults, Geological Survey and Mineral Exploration of Iran, Tehran.
Shirakova, E. I. (1967). General features in the orientation of principal stresses in earthquake foci in the Mediterranean-Asian seismic belt, Earth Phys., 1, 22-36.
Shrestha, B. and R. Tuladhar (2012). The response of Karnali Bridge, Nepal to near-fault earthquakes, Eng. Struct., 165, 4, 223-232.
Snyder, D. B. and M. Barazangi (1986). Deep crustal structure and flexure of the Arabian Plate beneath the Zagros collisional mountain belt as inferred from gravity observations. Tectonics, 5, 361-373.
Somerville, P. G. (2003). Magnitude scaling of the near fault rupture directivity pulse. Phys. Earth Planet. Int., 137, 201-212.
Somerville, P. G., N. F. Smith, R. W. Graves and N. A. Abrahamson (1997). Modification of empirical strong motion attenuation relations to include the amplitude and duration effect of rupture directivity, Seismol. Res. Lett., 68, 199-222.
Talebian, M. and J. Jackson (2002). Offset on the Main Recent Fault of NW Iran and implications for the late Cenozoic tectonics of the Arabia-Eurasia collision zone, Geophys. J. Int., 150, 422-439.
Tchalenko, J. S. and J. Braud (1974). Seismicity and structure of the Zagros (Iran): the Main Recent Fault between 33° and 35°N., Philos. Trans. R. Soc. Lond., 227, 1-25.
Tchalenko, J. S., J. Braud and M. Berberian (1974). Discovery of three earthquake faults in Iran, Nature, 248, 661-663.
Trifonov, V. G. (1978). Late Quaternary tectonic movements of western and central Asia. Geol. Soc. Am. Bull., 89, 7, 1059-1072.
Uhrhammer, R. (1986). Characteristics of Northern and Central California seismicity, Earthquake Notes, 57, 1, 21,
Vader, T. and C. C Daniel (2007). Influence of dampers on seismic response of cable-supported bridge towers, J. Bridge Eng., ISSN (print): 1084-0702.
Wells, D. L. and K. J. Coppersmith (1994). New empirical relationships among magnitude, rupture length, rupture width, rupture area, and surface displacement, Bull. Seismol. Soc. Am., 84, 974-1002.

***CORRESPONDING AUTHOR: Habib RAHIMI**,
Institute of Geophysics, Department of Earthquake seismology, Tehran, Iran
e-mail: rahimih@ut.ac.ir